

Selectivity mechanism of magnesium and calcium in cation-binding pocket structures of phosphotyrosine

Yusong Tu,^{1,2,*} Huadong Liu,^{3,*} Guosheng Shi^{4,*}, Fengmin Zhang,⁵ Tian Su^{6,3}, Yuanyan Wu,¹ Jiajia Sun,¹ Lei Zhang,⁶ Shengli Zhang,^{6,†} and Haiping Fang^{6,7,8,‡}

¹College of Physics Science and Technology, Yangzhou University, Jiangsu 225009, China

²Key Laboratory of Polar Materials and Devices, Ministry of Education, College of Physics and Electronic Science, East China Normal University, Shanghai 200062, China

³Center for Mitochondrial Biology and Medicine, The Key Laboratory of Biomedical Information Engineering of Ministry of Education, School of Life Science and Technology, Xi'an Jiaotong University, Xi'an 710049, China


⁴Shanghai Applied Radiation Institute, Shanghai University, Shanghai 200444, China

⁵Testing Center, Yangzhou University, Jiangsu 225009, China

⁶MOE Key Laboratory for Nonequilibrium Synthesis and Modulation of Condensed Matter, School of Science, Xi'an Jiaotong University, Xi'an 710049, China

⁷Division of Interfacial Water and Key Laboratory of Interfacial Physics and Technology, Shanghai Institute of Applied Physics, Chinese Academy of Sciences, Shanghai 201800, China

⁸School of Science, East China University of Science and Technology, Shanghai 200237, China

 (Received 12 September 2019; revised manuscript received 26 December 2019; accepted 27 January 2020; published 14 February 2020)

Magnesium (Mg^{2+}) and calcium (Ca^{2+}) are of essential importance in biological activity, but the molecular understanding of their selectivity is still lacking. Here, based on density functional theory calculations and *ab initio* molecular dynamics simulations, we show that Mg^{2+} binds more tightly to phosphotyrosine (pTyr) and stabilizes the conformation of pTyr, while Ca^{2+} binds more flexibly to pTyr with less structural stability. The key for the selectivity is attributed to the cation- π interactions between the hydrated cations and the aromatic ring together with the synergic interaction between the cations and the side groups in pTyr to form a cation-binding pocket structure, which we refer as *side-group-synergetic hydrated cation- π interaction*. The existence and relative strength of the cation- π interactions in the pocket structures as well as their structural stability have been demonstrated experimentally with ultraviolet (UV) absorption spectra and ^1H NMR spectra. The findings offer insight into understanding the selectivity of Mg^{2+} and Ca^{2+} in a variety of biochemical and physiological essential processes.

DOI: [10.1103/PhysRevE.101.022410](https://doi.org/10.1103/PhysRevE.101.022410)

I. INTRODUCTION

Magnesium (Mg^{2+}) and calcium (Ca^{2+}) are both of essential importance for a variety of biochemically and physiologically essential processes in life, including signaling, enzyme activation, and catalysis [1–3]. Although both Mg^{2+} and Ca^{2+} are alkaline earth divalent cations, proteins generally acquire specific ions for biological functions [4–6]. Mg^{2+} is an essential catalytic cofactor in a number of enzyme families, e.g., for many phosphate transfer reactions [4], and Ca^{2+} is a ubiquitous signal responsible for controlling numerous cellular processes [7], nevertheless, Mg^{2+} and Ca^{2+} also face stiff competitions for their specific binding sites in proteins [6,8–12]. For example, Mg^{2+} binding in DNA and RNA polymerases is crucial for catalysis in DNA synthesis and editing functions [13,14], and Ca^{2+} is found to bind consistently to the active site for activity inhibition [15,16]. Generally, catalysis reactions necessitate conformational stability in transition

states of substrate proteins, and biological signaling processes demand conformational changes or switches of proteins for signal transduction. Herein, an essential question regarding the selectivity of Mg^{2+} and Ca^{2+} is whether or to what extent Mg^{2+} and Ca^{2+} exert the characteristics of conformational stabilization and triggering conformational changes or switches, respectively, in their biological activity.

Tyrosine (Tyr, one of three essential aromatic amino acids) and phosphotyrosine (pTyr), as well as their interactions with Mg^{2+} and Ca^{2+} ions, have been known to play crucial roles in the essential phosphorylation controlling cell proliferation, differentiation, migration, and immune response [17–20]. Mg^{2+} is found to catalyze phosphate-transfer reactions on Tyr residues to become pTyr in Tyr phosphorylation [21–23], and Ca^{2+} dependence is also observed in the conformational changes of the protein domain [Src homology 2 (SH2)] bound by pTyr [24]. However, so far, not only are the different behaviors of $\text{Mg}^{2+}/\text{Ca}^{2+}$ in biological activity not understood but also the exact role of $\text{Mg}^{2+}/\text{Ca}^{2+}$ in Tyr phosphorylation remains unclear.

Here, we examine the interaction of pTyr with $\text{Mg}^{2+}/\text{Ca}^{2+}$ as an example to understand the $\text{Mg}^{2+}/\text{Ca}^{2+}$ selectivity in

*These authors contributed equally to this work.

†zhangsl@xjtu.edu.cn

‡fanghaiping@sinap.ac.cn

a variety of biochemical and physiological processes. We show that Mg^{2+} binds more tightly to pTyr to stabilize the conformation of pTyr, while Ca^{2+} binds more flexibly to pTyr with less structural stability, based on our density functional theory (DFT) calculations and *ab initio* molecular dynamics (AIMD) simulations. The difference of the stability, namely the $\text{Mg}^{2+}/\text{Ca}^{2+}$ selectivity, of cation-binding structures in pTyr is attributed to the cation- π interactions between the hydrated cations and the aromatic ring together with the synergic interaction between the cations and the side groups in pTyr to form a cation-binding pocket structure. Here we refer to the interaction as *side-group-synergetic hydrated cation- π interaction*. The existence and relative strength of the cation- π interactions in the pocket structures as well as their structural stability have been demonstrated experimentally with ultraviolet (UV) absorption spectra and ^1H NMR spectra. It should be noted that the synergetic interaction of side groups with the cations greatly enhances the stability of the $\text{Ca}^{2+}/\text{Mg}^{2+}$ on the aromatic rings; without synergetic side groups, e.g., the phosphate group, the structures of Tyr for cation binding become unstable and cations are easily dispersed away from Tyr. To the best of our knowledge, such side-group-synergetic hydrated cation- π interaction has not been reported previously. The findings are also of fundamental importance and provide insight into understanding the selectivity of Mg^{2+} and Ca^{2+} in a variety of biochemically and physiologically essential processes.

II. METHODS

Computer simulation methods. The AIMD simulations were performed with the CP2K 4.1 packages [25]. We adopt a hybrid Gaussian and plane waves [26] or Gaussian and augmented plane waves (GAPW) [27] scheme to DFT implemented in the subroutine QUICKSTEP [28], and the electronic density is expanded in the form of plane waves with a cutoff of 280 Ry. The GAPW scheme is only applied for Mg^{2+} and Ca^{2+} ions to achieve well-converged forces. Goedecker-Teter-Hutter pseudopotentials [29] are used to represent the core electrons, and only the valence electrons are considered explicitly; e.g., the semicores of Mg^{2+} and Ca^{2+} are treated explicitly, which involves ten valence electrons. Double-zeta split valance basis sets are used for all atomic kinds. We use revised Perdew-Burke-Ernzerhof (revPBE) [30] for the exchange and correlation functional. Grimme D3 dispersion corrections are used [31]. Previous studies have shown that better bulk water properties could be achieved with the choice of revPBE-D3 protocol [32–35]. In AIMD simulations, the self-consistent field convergence criterion is chosen as 10^{-6} a.u. The *NVT* ensemble is used with a time step of 0.5 fs and the temperature is maintained at 300 K by a Nosé-Hoover thermostat with a time constant of 0.5 ps.

The geometry structures for pTyr with $\text{Mg}^{2+}/\text{Ca}^{2+}$ were obtained by DFT optimization calculations, at the B3LYP/6-31+G(d,p) level of theory [36] by using the GAUSSIAN-09 package [37]. As the convergence criteria, the maximum step size is 0.0018 a.u. and the root-mean-square (RMS) force is 0.0003 a.u. Explicit hydration water molecules surrounding cations were considered, and the polarizable continuum model (PCM) model was applied as aqueous background

environment. Furthermore, the whole optimized geometry structures achieved by DFT calculations were transferred to a cubic box with a side length of 16.56 Å filled with 128 water molecules, which corresponds to be a density of ~ 1 g/ml, and Cl^- ion were introduced as opposite charge for the whole system neutralization. Multiple steps were applied to reoptimize the whole systems. We first performed the classic molecular dynamics simulations to equilibrate the systems with the frozen structure of pTyr with the cation for periods of 10 ns using the SPC/E water model and OPLS (optimized potential for liquid simulations) force field for the ions. Then, we fixed the structures of pTyr with the cation and then released them to successively twice perform the global geometry optimizations of the systems with the CP2K 4.1 packages. The eventual optimized systems were applied as the initial structures to run AIMD simulations.

Experiments materials. The O-phospho-L-tyrosine (pTyr, 99%), magnesium chloride (MgCl_2 , 98%), and calcium chloride (CaCl_2 , 96%) powders were purchased from J&K Scientific Ltd. All samples were used without purification and preprocessing. All salt solutions and pTyr solutions were prepared with 18.2 MΩ, 3 ppb TOC Milli-Q water (Millipore, US).

UV spectroscopy. UV absorption spectra of pTyr, MgCl_2 , CaCl_2 , Mg^{2+} -pTyr, and Ca^{2+} -pTyr solutions were recorded on a U-3900 spectrophotometer (Hitachi, Japan). The pTyr solutions had an initial concentration of 0.0006 mol/l. The pTyr solution and the $\text{CaCl}_2/\text{MgCl}_2$ solution were mixed together with a volume ratio of 1:1 to achieve the pTyr concentration of 0.0003 mol/l and the relevant various concentrations of $\text{CaCl}_2/\text{MgCl}_2$ in UV spectra experiments.

^1H NMR experiments. All ^1H NMR experiments were performed at 298 K. ^1H NMR spectra were recorded on a Bruker AVANCE spectrometer operating at 600.23 MHz ^1H resonance frequency. 90% H_2O and 10% D_2O were used as solvent. A noesygppr1d pulse sequence was applied to suppress the water signal. A slender sealed capillary filled with deuterated dimethyl sulfoxide (DSMO- d_6) was placed inside the sample tubes, and the DSMO signal was adopted as an external reference to quantify the chemical shifts of the samples. The pTyr solution had an initial volume of 400 μl and an initial concentration of 0.0003 mol/l, and the ion concentrations (~ 0.003 , ~ 0.006 , ~ 0.01 , ~ 0.02 , ~ 0.033 , and ~ 0.05 mol/l) were achieved by adding the corresponding volumes (10, 25, 50, 100, 200, and 400 μl) of the ion solution with an initial concentration of 0.1 mol/l into the pTyr solution, respectively.

III. RESULTS AND DISCUSSION

We first performed DFT calculations at the B3LYP/6-31+G(d,p) level of theory to obtain the optimized geometry structure for pTyr with $\text{Mg}^{2+}/\text{Ca}^{2+}$, using explicit hydration water around the cation and polarizable continuum model (see detailed methods in the Supplemental Material (SM) [38]). Figure 1 shows the optimized structures ($t = 0$ ps). We can see that the cation is embraced by the aromatic ring and the side groups of pTyr. In other words, the aromatic ring and the side groups form a pocket structure for the cation. The average distances between the cations and the aromatic

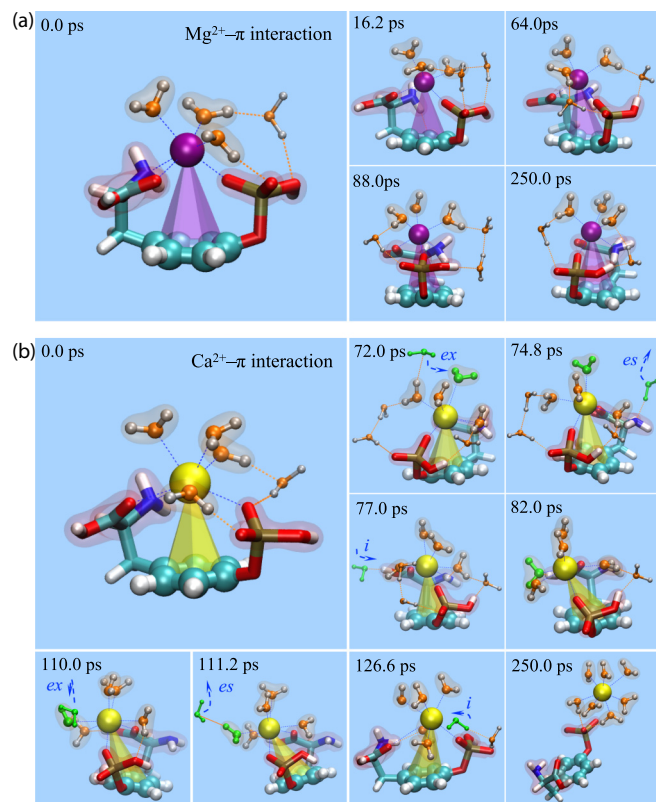


FIG. 1. Cation-binding pocket of phosphotyrosine (pTyr) and side-group-synergetic hydrated cation- π interactions. Representative AIMD trajectories of the conformations in the pocket structures of pTyr for Mg^{2+} (a) and Ca^{2+} (b), respectively. The numbers indicate the time of snapshots. The structures at $t = 0$ ps are achieved by geometry optimization with DFT calculations. The aromatic ring in pTyr are shown as big bonded spheres, the side groups as bonded sticks, and $\text{Mg}^{2+}/\text{Ca}^{2+}$ as a sphere (C: cyan; N: blue; O: red; H: white; Mg: purple; and Ca: yellow), and the surfaces of side groups, i.e., the carboxyl, amino and phosphate groups, are shown in pale red. The first-shell waters, whose oxygens do not exceed 2.8 \AA from the cation, are shown as bonded spheres with their surfaces shown in pale pink, and the waters that are hydrogen-bonded with the phosphate group and the first-shell water are shown as small bonded spheres, (O: pink; H: grey), and the other waters are omitted for a clear view. The cations and their first-shell water and the key atoms in the side groups are linked by blue dashed lines, and the hydrogen bonds by pink dashed lines. The transparent six-face cones (purple, yellow) comprising the cation (Mg^{2+} , Ca^{2+}) and six aromatic-carbon atoms are indicative of the cation- π interaction. In (b), the wholly green molecules represent the intruding (*i*), exchanging (*ex*), or escaping (*es*) water molecules within the hydration water around the Ca^{2+} ion, with the blue dashed arrows indicating the *i*, *ex*, and *es* directions.

ring were computed: 4.14 and 3.78 \AA respectively for Mg^{2+} and Ca^{2+} [see Figs. 2(a) and 2(b)]. These distances fall into the distance ranges between cations and aromatic ring with cation- π interaction [39–41], indicating the existence of cation- π interaction between $\text{Mg}^{2+}/\text{Ca}^{2+}$ and the aromatic ring structure of pTyr [41,42]. Moreover, the average distances between the cation and the key atoms in side groups, i.e., carbonyl oxygen, amino nitrogen, and phosphate oxygen near the cation, are in the ranges of $\sim 2.1\text{--}2.3 \text{ \AA}$ and $\sim 2.5\text{--}2.8 \text{ \AA}$

respectively for Mg^{2+} and Ca^{2+} [see Fig. 2(f)], showing that the cations are bound to the side groups [43,44].

Further, we performed AIMD simulations for this system to exploit the stability of the pocket structures in a full explicit water environment. Two representative AIMD trajectories are shown in Fig. 1 (see also Movies S1 and S2 in SM). In Fig. 1(a), we can see that the pocket structure of pTyr for Mg^{2+} is maintained during the whole simulation of 250 ps. The conformation in this pocket structure is kept very stable. As shown in the snapshots at 16.2, 64.0, 88.0, and 250.0 ps, there is no apparent variation in the conformation, although we can see clear rearrangement of the positions with dynamical orientations of the water surrounding the Mg^{2+} . As shown in Fig. 2(a), the distances between the Mg^{2+} and the center of the aromatic ring have only a small fluctuation around the average value of 4.14 \AA over time. These distances fall into the range between cations and the aromatic ring with cation- π interaction [39–41]. Figure 2(d) presents the distribution of the deflection angle between the link line of cation and aromatic ring and the normal direction of the aromatic ring in the pocket structure of pTyr for Mg^{2+} . This distribution also has only a narrow deviation from zero angle. The average root-mean-square deviation (RMSD) of the pocket structure is just $\sim 0.3 \text{ \AA}$ relative to the initial structure [Fig. 2(e)]. These results indicate the existence of the Mg^{2+} - π interaction as well as the stability of the pocket structure. In contrast, as shown in Fig. 1(b), the pocket structure of pTyr for Ca^{2+} is only maintained in the first ~ 126 ps. Interestingly, a conformational switch is observed in this pocket structure. Within the first 72 ps, there is a conformation of the pocket structure formed by the carbonyl, amino, and phosphate side groups and the aromatic ring, very similar to the pocket for Mg^{2+} . The conformation is denoted as conformation I. After 82 ps, a different conformation of the pocket structure is constituted only by the carbonyl, hydroxyl and phosphate groups while the amino group stays away from the Ca^{2+} . The latter conformation is denoted as conformation II (see the snapshots at 82.0, 110.0, 111.2 ps). Figure 2(b) shows the distances between the Ca^{2+} and the aromatic ring with time. These distances present a two-step profile with the average values of 3.78 and 4.38 \AA , corresponding to the distances in conformations I and II, respectively. All distances also fall into the range between cations and aromatic ring with cation- π interaction [39–41], indicating the existence of Ca^{2+} - π interactions. We denote the cation- π interactions in these two conformations as Ca^{2+} - π (I) and Ca^{2+} - π (II), respectively. In Figs. 2(d) and 2(e), we also see the two-step behaviors of both the deflection angles and the RMSDs, respectively, with their probability distributions around 0° and 18° , and with the average RMSD values of $\sim 0.6 \text{ \AA}$ and $\sim 0.9 \text{ \AA}$ relative to the initial structure. In addition, the conformational variations observed in the pocket structure are also reflected in the exchanging or intruding behaviors of water molecules surrounding Ca^{2+} [see the snapshots of 72, 82, and 110 ps in Fig. 1(b) and also Movie S2 in SM].

The stability of cation-binding pocket structures in pTyr is attributed to the cation- π interactions between the hydrated cations and the aromatic ring in pTyr together with the interaction between the cations and synergic side groups in pTyr. The distances from the cation to the aromatic ring increase

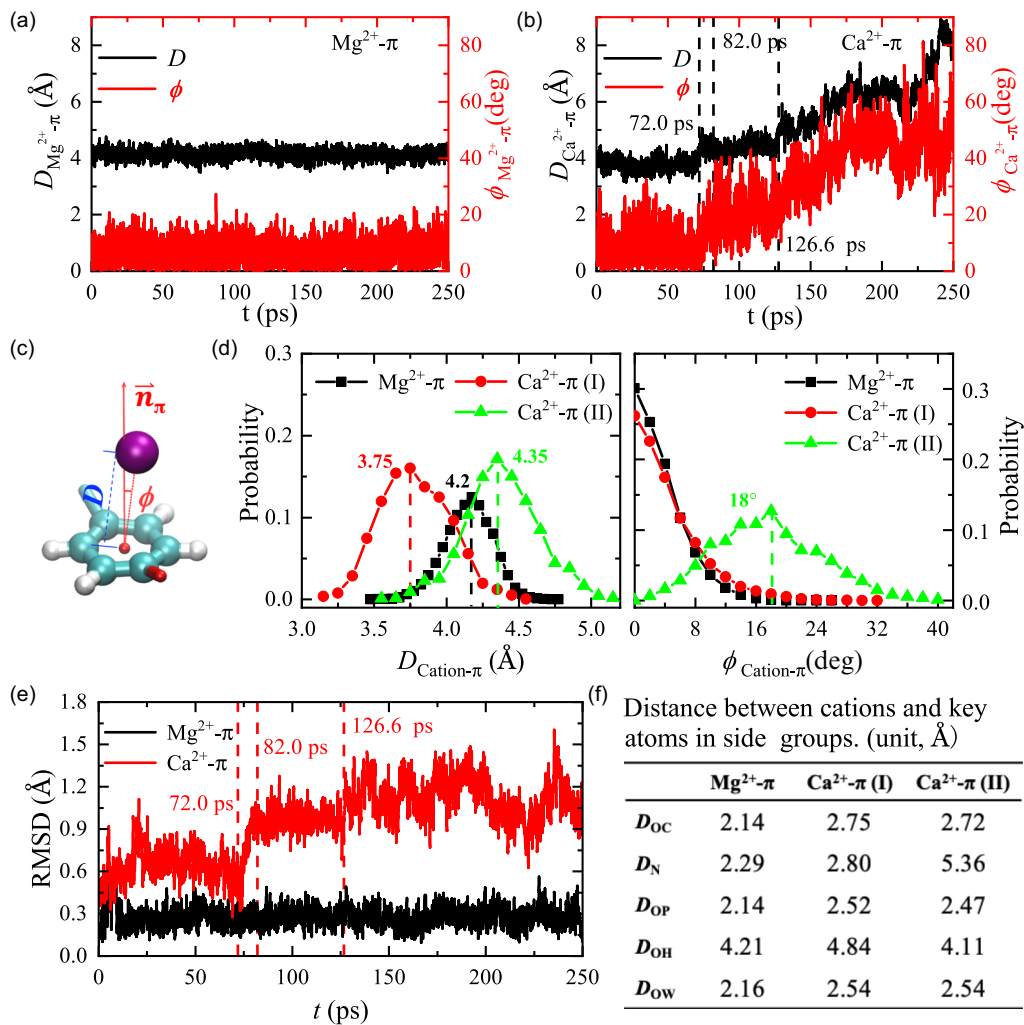


FIG. 2. Structural variables of side-group-synergetic hydrated cation- π interactions. (a) and (b) Time evolution of the distances and deflection angles between the cation and the aromatic ring for both representative trajectories shown in Fig. 1. Three vertical lines indicate the times 72.0, 82.0, and 126.6 ps in (b) and also in (e). (c) Definition diagram of structural variables. D is the distance of the link line between the cation and the center of aromatic ring. ϕ is the polar angle between the link line and the normal direction of aromatic ring plane (\vec{n}_π). The red small sphere marks the position of the center of the aromatic ring, and atom representations and color settings are as in Fig. 1. (d) Probability distributions of $D_{cation-\pi}$ and $\phi_{cation-\pi}$. The data within the whole 250 ps of the trajectory with Mg^{2+} and the data within [0,72] ps and [82,126.6] ps of the trajectory with Ca^{2+} are adopted to obtain the distributions for $Mg^{2+}-\pi$, $Ca^{2+}-\pi$ (I) and $Ca^{2+}-\pi$ (II) interactions, respectively. The most probable values are indicated by relevant vertical lines and numbers. (e) Root-mean-square deviation (RMSD) of all atoms except for hydrogen atoms in the pocket structures of pTyr in both representative trajectories. RMSDs are calculated relative to the structures at $t = 0$ ps. (f) Average distances with $Mg^{2+}-\pi$, $Ca^{2+}-\pi$ (I) and $Ca^{2+}-\pi$ (II) interactions. D_{OC} , D_{OH} , D_N , D_{OP} , and D_{OW} correspond to the distances between cations and the key atoms in side groups, i.e., carbonyl oxygen, hydroxyl oxygen, amino nitrogen, phosphate oxygen near cations, and the oxygen of the first-shell water around cations, respectively.

in the order $Ca^{2+}-\pi(I) < Mg^{2+}-\pi < Ca^{2+}-\pi(II)$. We suggest the order from strong to weak strength is $Ca^{2+}-\pi(I) > Mg^{2+}-\pi > Ca^{2+}-\pi(II)$, considering that in general the shorter the interacting distance is between cation and aromatic ring structure, the stronger the cation- π interaction is [39–41]. On the other hand, the side groups in pTyr likewise play a critical role in the stability of the pockets. The distances of the key atoms in side groups of pTyr from Mg^{2+} (~ 2.1 – 2.3 Å) are much shorter than the distances from Ca^{2+} (~ 2.5 – 2.8 Å) in conformation I [see Fig. 2(f)], indicating the tighter binding of side groups with Mg^{2+} than with Ca^{2+} . In conformation II, the Ca^{2+} is on average 5.36 Å from the nitrogen [see Fig. 2(f)],

about twice of the distances from the Ca^{2+} to other key atoms in the side groups, indicating that the amino group is away from the Ca^{2+} [see snapshots after 82 ps, Fig. 1(b)].

To further analyze the side-group-synergetic hydrated cation- π interactions, on the basis of the optimized geometries of pTyr with the cations [Figs. 1(a) and 1(c)], we divided the pocket structure into two parts, i.e., the pTyr and the hydrated cation, and then performed single-point calculations at the B3LYP/TZ2P level of theory in the framework of DFT in the ADF program and decomposed the interaction energies between these two parts. As shown in Table S1, the total interaction energies between pTyr and the hydrated cation

were decomposed into Pauli repulsion, orbital interaction, and electrostatic interaction using an energy decomposition analysis (EDA). The EDA results show that the electrostatic interactions and orbital interactions supply the main interaction energy, and the Pauli repulsion affords the main repulsive energy. Moreover, also regarding optimized geometries, we analyzed the molecular orbitals, and the highest occupied molecular orbital (HOMO) in the pocket structure is shown in Fig. S1. We can observe the clear coupling of the electrons of oxygen atoms in water, the electrons of side groups, and the delocalized π ring in pTyr and empty orbitals of Mg^{2+} and Ca^{2+} . Likewise, we have estimated, based on the optimized geometries, the binding energy of $\text{Mg}^{2+}/\text{Ca}^{2+}$ in the pocket structure of pTyr. We pulled the cation away from the optimized structures of pTyr to infinity and carried out the single-point calculations, showing the required energies equal to -131.2 and $-178.1 \text{ kcal mol}^{-1}$, respectively in the pocket structure of pTyr with Mg^{2+} and Ca^{2+} . Meanwhile, the relevant Mulliken charges of the atoms of the aromatic ring in the optimized structures of pTyr are shown in Fig. S2. We can indeed see the significant changes of these local charges (the maximal change is up to $0.173e$), compared with the charges in the corresponding structure where the cation was pulled away to infinity. All these analyses indicate that the side-group-synergetic hydrated cation- π interactions between $\text{Mg}^{2+}/\text{Ca}^{2+}$ and the aromatic ring in pTyr greatly enhances the stability of cation-binding pocket structures in pTyr.

To further analyze the role of the synergic side groups, we considered the Mulliken charges in the optimized structures and explicitly estimated the electrostatic interactions between the $\text{Mg}^{2+}/\text{Ca}^{2+}$ and the phosphate groups, i.e., respectively. The electrostatic energies of the phosphate groups with Mg^{2+} and Ca^{2+} are -45.8 and $-81.9 \text{ kcal mol}^{-1}$, respectively, indicating the significant contribution of the phosphate groups in the formation of the pocket structure of pTyr with the cation. Furthermore, we removed the synergic side groups, e.g., the phosphate group, and performed DFT calculations to analyze the interaction between $\text{Ca}^{2+}/\text{Mg}^{2+}$ and Tyr. The same optimization and equilibration processes as in the systems with pTyr were applied in the DFT calculations and the AIMD simulations. Figure 3 presents two representative AIMD trajectories and Fig. 4 shows the distances and the deflection angles of cation- π interactions between Tyr and $\text{Mg}^{2+}/\text{Ca}^{2+}$. We see that the structures of Tyr for cation binding easily become unstable and cations are dispersed away from Tyr into the water solution within a dozen picoseconds, which is consistent with the above analyses. Last, we also have investigated the structure of pTyr with a Na^+ ion. As shown in Fig. S3 and S4, we see that the structure between pTyr and Na^+ is maintained for only ~ 16 ps. This indicates that the structures between pTyr and divalent ions are much more stable than the structures between pTyr and monovalent ions.

Experimentally, ultraviolet (UV) absorption spectral experiments were performed to show evidence of the cation- π interactions between $\text{Mg}^{2+}/\text{Ca}^{2+}$ and the aromatic ring structure in pTyr. In order to quantify the influence of cation- π interaction on UV absorption spectrum, the UV absorbance difference spectrum is determined with the UV absorbance spectrum of pure pTyr solution *plus* the spectrum

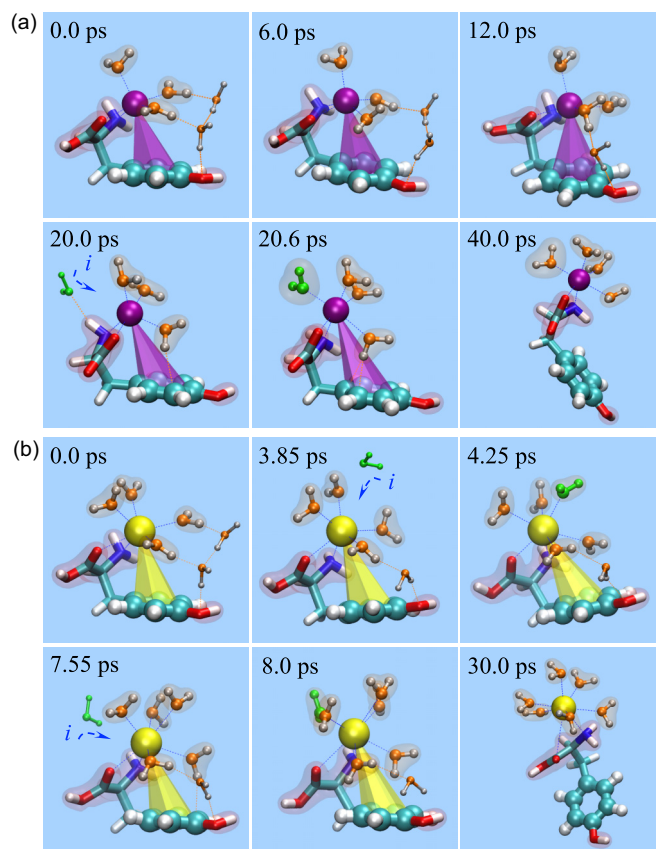


FIG. 3. Cation-binding structures of Tyr for $\text{Mg}^{2+}/\text{Ca}^{2+}$. Representative AIMD trajectories of the conformations of Tyr with Mg^{2+} (a) and Ca^{2+} (b), respectively. The numbers indicate the times of snapshots. Atom representations and color settings are as in Fig. 1.

of pure $\text{CaCl}_2/\text{MgCl}_2$ solution *minus* the spectrum of the pTyr solution with addition of the $\text{CaCl}_2/\text{MgCl}_2$ solution. In Fig. S6, we clearly see the absorbance difference peaks that occur at $\sim 230 \text{ nm}$ in the UV absorbance difference spectra, which are assigned to a conjugate double bond of the aromatic group that easily generated the π - π^* transition [45–47]. Figure 5(a) shows the dependence of these peaks at $\sim 230 \text{ nm}$ on cations concentrations. We find that these peaks at $\sim 230 \text{ nm}$ are enhanced markedly increasing cation concentration ($>0.02 \text{ mol/l}$) increasing. The marked enhancement indicates that the conjugate double bonds of the aromatic group in pTyr are greatly affected by the addition of various salt solutions. Notably, analogous UV difference spectra in relation to the cation- π interactions have been observed previously for the aromatic ring structures in graphene oxide [47] as well as a tryptophan [46] and an indolyl model compound (Gly-Asn-His-Trp-NH₂) [48]. The similarity between the peaks at $\sim 230 \text{ nm}$ in UV difference spectra observed here and those reported earlier indicates the existence of the cation- π interaction between $\text{Mg}^{2+}/\text{Ca}^{2+}$ and the aromatic ring structure in pTyr. More interestingly, the peaks at $\sim 230 \text{ nm}$ induced by the addition of CaCl_2 solution are always larger than those induced by the addition of MgCl_2 solution at the same cation concentrations. This indicates a stronger cation- π interaction between Ca^{2+} and the aromatic ring structure in pTyr, consistent with the theoretical result above.

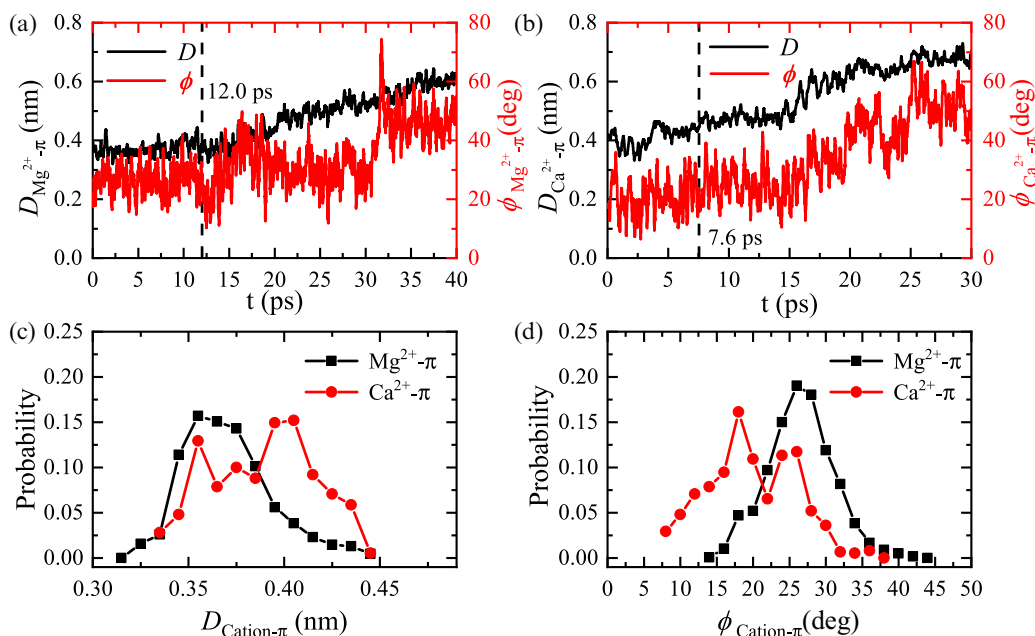


FIG. 4. Cation- π distances and deflection angles. (a) and (b) Time evolution of cation- π distances (D , black) and deflection angles (ϕ , red) for both representative trajectories shown in Fig. 3. (c) and (d) Probability distributions of D and ϕ for both cation- π interactions. The data within the first 12.0 and the 7.6 ps are adopted to obtain the distributions for Mg^{2+} - π and Ca^{2+} - π interactions, respectively.

^1H NMR experiments were further carried out to analyze the cation- π interactions between $\text{Mg}^{2+}/\text{Ca}^{2+}$ and the aromatic ring structure in pTyr as well as their structural stability. As shown in Fig. 5(b), without $\text{MgCl}_2/\text{CaCl}_2$ (zero concentration), the chemical shifts (δ_H) of four hydrogen atoms on the typical para-disubstituted aromatic ring of pTyr present two groups of bimodal peaks in ^1H NMR spectra, consistent with previous experiments and analyses of para-disubstituted benzene compounds [49,50]. Importantly, we clearly see the chemical shift variations ($\Delta\delta_H$) in ^1H NMR spectra induced by addition of $\text{MgCl}_2/\text{CaCl}_2$ solution. We ascribe these $\Delta\delta_H$ to the influence from the cation- π interactions between $\text{Mg}^{2+}/\text{Ca}^{2+}$ and the aromatic ring structure. Figure 5(c) shows the dependence of $\Delta\delta_H$ on cation concentrations. Both $\Delta\delta_H$ increase gradually with increasing $\text{MgCl}_2/\text{CaCl}_2$ concentrations. Interestingly, at very low concentrations, the $\Delta\delta_H$ induced by MgCl_2 are comparable to the $\Delta\delta_H$ by CaCl_2 . After ~ 0.01 mol/l, the $\Delta\delta_H$ induced by CaCl_2 increases rapidly and becomes significantly larger than the $\Delta\delta_H$ induced by MgCl_2 ; in contrast, the $\Delta\delta_H$ induced by MgCl_2 is maintained at relatively small values and after ~ 0.033 mol/l starts to increase rapidly. The significantly larger influence on the $\Delta\delta_H$ induced by CaCl_2 indicates a stronger cation- π interaction between Ca^{2+} and the aromatic ring structure in pTyr than that between Mg^{2+} and the aromatic ring structure, consistent with the theoretical result above. Moreover, in Fig. 5(b), these two groups of split bimodal peaks in ^1H NMR spectra present inconsistent $\Delta\delta_H$, especially at high cation concentrations, indicating the asymmetrical influence from $\text{MgCl}_2/\text{CaCl}_2$ on four hydrogen atoms on the the para-disubstituted aromatic ring of pTyr. The asymmetrical influence induced by CaCl_2 is much more significant than that induced by MgCl_2 . This also indicates more significant

deviation of Ca^{2+} from the normal direction of the aromatic ring and consequently less structural stability in the pocket structures of pTyr for Ca^{2+} , in comparison with the case in the pocket structure of pTyr for Mg^{2+} . Here, the strength relation of cation- π interactions indicated in ^1H NMR spectra is consistent with both the theoretical result and the experimental result in UV absorption spectra above, and the greater structural stability of Mg^{2+} - π interactions in pTyr indicated in ^1H NMR spectra is also consistent with the theoretical result.

Meanwhile, based on the optimized geometries [Figs. 1(a) and 1(c)], we also used the time-dependent density functional theory (TDDFT) to calculate the UV adsorption spectra and adopted the gauge independent atomic orbital (GIAO) method to analyze the NMR spectra (see Methods section). To estimate the influence of the cations in the pocket structure of pTyr on both spectra, we pulled the cation away from the optimized structures of pTyr to infinity. As shown in Fig. S5A and S5B, we compare the calculated UV spectra of pTyr without the cation and with the cation. We see that the spectra in pTyr with the cations are much lower than the spectra in pTyr without the cations. This contrast suggests that the suppressed tendency is caused by the cation- π interaction in the pocket structure of pTyr with the cation, consistent with our UV experiments above. Similarly, Fig. S5C and S5D present the chemical shifts of four hydrogen atoms of the aromatic ring for pTyr and for pTyr with the cation, and all the chemical shifts are shifted downfield. The downfield-shifted tendency is consistent with our NMR experiments. These calculated spectra indicate that the experimental UV absorbance difference spectrum and chemical shift variations indeed originate from the cation- π interactions between $\text{Mg}^{2+}/\text{Ca}^{2+}$ and the aromatic ring structure in pTyr.

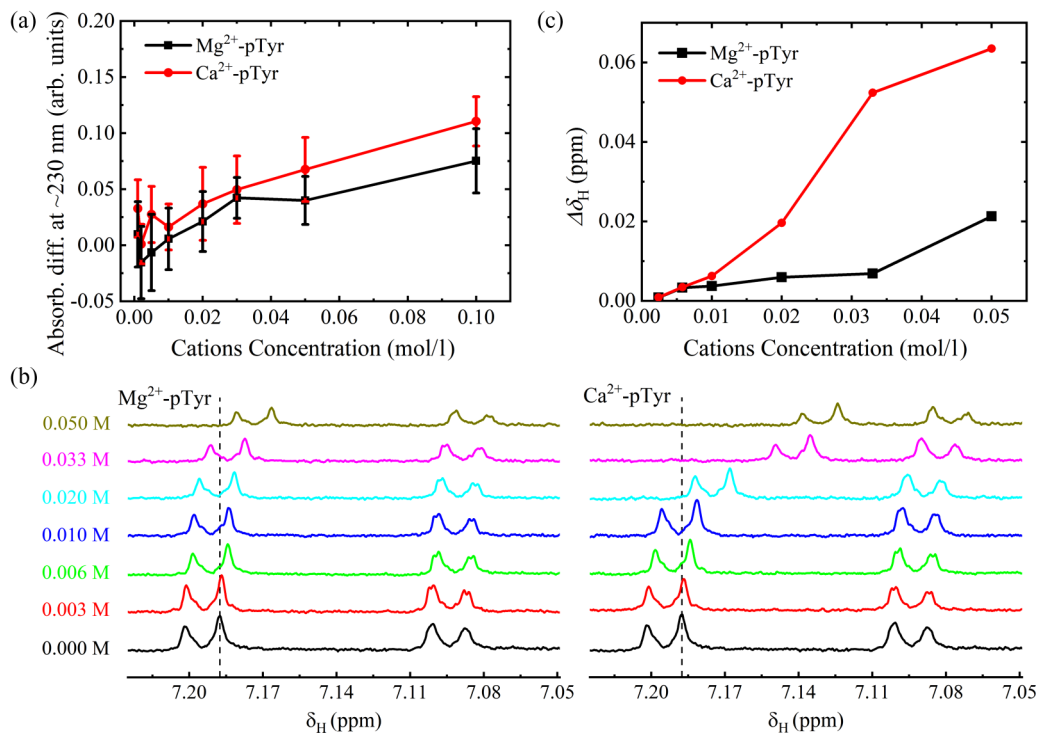


FIG. 5. Experimental evidence of side-group-synergetic hydrated cation- π interactions. (a) Dependence of UV absorbance difference at ~ 230 nm on cation concentrations. UV absorbance difference spectrum is determined with the UV absorbance spectrum of pure pTyr solution *plus* the spectrum of pure CaCl₂/MgCl₂ solution *minus* the spectrum of the pTyr solution with addition of the CaCl₂/MgCl₂ solution. Error bars indicate the standard deviation from three parallel experiments. (b) and (c) Chemical shifts (δ_H) as well as chemical shift variations ($\Delta\delta_H$) of the hydrogen atoms on the aromatic ring of pTyr in ^1H NMR spectra, induced by addition of CaCl₂/MgCl₂ with various concentrations. In (b), two groups of split bimodal peaks (δ_H) in ^1H NMR spectra correspond to four hydrogen atoms on the para-disubstituted aromatic ring of pTyr, and the numbers correspond to cation concentrations. $\Delta\delta_H$ in (c) is estimated as the peak δ_H marked by dashed lines *minus* the δ_H at zero cation concentration in (b).

IV. CONCLUSION

In summary, we have examined the interacting of pTyr with Mg²⁺ and Ca²⁺ and we have shown the clear selectivity for Mg²⁺ over Ca²⁺ in the cation-binding structures of pTyr; i.e., Mg²⁺ binds more tightly to pTyr to stabilize the conformation of pTyr, while Ca²⁺ binds more flexibly to pTyr with less structural stability. We attribute the selectivity of cation-binding structures of pTyr to the pocket structure formation due to the *side-group-synergetic hydrated cation- π interaction* between the hydrated Mg²⁺ or Ca²⁺ and the aromatic ring structure. UV absorption spectra and ^1H NMR spectra demonstrate the existence and relative strength of cation- π interactions in the pocket structures of pTyr for Mg²⁺/Ca²⁺ as well as their structural stability, consistent with the theoretical result.

It should be noted that we show that the synergetic interaction of side groups with the cations greatly enhances the stability of the Ca²⁺/Mg²⁺ on the aromatic rings in aqueous solution, in addition to the cation- π interactions. Our theoretical computations have shown that, without synergetic

side groups, e.g., the phosphate group, the structures of Tyr for cation binding easily become unstable and cations are dispersed away from Tyr into the water solution within a dozen picoseconds. Thus, our study demonstrates essentially how to achieve cation- π interactions for relevant biological aromatic residues of proteins in biological systems, and the side-group-synergetic hydrated cation- π interactions might become the pivotal factor for cation bioactivity and relevant functions in biological systems. The findings also offer insight into understanding the selectivity of Mg²⁺ and Ca²⁺ in a variety of biochemical and physiological essential processes.

ACKNOWLEDGMENTS

Support from the National Natural Science Foundation of China (Grants No. 11675138, No. 11705160, and No. 11774280), the National Science Fund for Outstanding Young Scholars (Grant No. 11722548), the Special Program for Applied Research on Supercomputation of the NSFC-Guangdong Joint Fund (the second phase), and the Supercomputer Center of CAS is acknowledged.

[1] J. A. Cowan, *Biological Chemistry of Magnesium* (Wiley-VCH, Weinheim, 1995).

[2] E. Carafoli and C. B. Klee, *Calcium as a Cellular Regulator* (Oxford University Press, Oxford, 1999).

- [3] R. Smith, Calcium and bacteria, *Adv. Microb. Physiol.* **37**, 83 (1995).
- [4] J. A. Cowan, Metal activation of enzymes in nucleic acid biochemistry, *Chem. Rev.* **98**, 1067 (1998).
- [5] M. J. Berridge, M. D. Bootman, and P. Lipp, Calcium—a life and death signal, *Nature (London)* **395**, 645 (1998).
- [6] T. Dudev and C. Lim, Competition among metal ions for protein binding sites: Determinants of metal ion selectivity in proteins, *Chem. Rev.* **114**, 538 (2013).
- [7] M. J. Berridge, P. Lipp, and M. D. Bootman, The versatility and universality of calcium signalling, *Nat. Rev. Mol. Cell Biol.* **1**, 11 (2000).
- [8] R. E. White and H. C. Hartzell, Effects of intracellular free magnesium on calcium current in isolated cardiac myocytes, *Science* **239**, 778 (1988).
- [9] J. Shi, G. Krishnamoorthy, Y. Yang, L. Hu, N. Chaturvedi, D. Harilal, J. Qin, and J. Cui, Mechanism of magnesium activation of calcium-activated potassium channels, *Nature (London)* **418**, 876 (2002).
- [10] L. T. Iseri and J. H. French, Magnesium: nature’s physiologic calcium blocker, *Am. Heart J.* **108**, 188 (1984).
- [11] C. Toyoshima, S. Iwasawa, H. Ogawa, A. Hirata, J. Tsueda, and G. Inesi, Crystal structures of the calcium pump and sarcoplipin in the Mg^{2+} -bound E1 state, *Nature (London)* **495**, 260 (2013).
- [12] M. J. Knape, L. G. Ahuja, D. Bertinetti, N. C. Burghardt, B. Zimmermann, S. S. Taylor, and F. W. Herberg, Divalent metal ions Mg^{2+} and Ca^{2+} have distinct effects on protein kinase A activity and regulation, *ACS Chem. Biol.* **10**, 2303 (2015).
- [13] C. A. Brautigam and T. A. Steitz, Structural and functional insights provided by crystal structures of DNA polymerases and their substrate complexes, *Curr. Opin. Struct. Biol.* **8**, 54 (1998).
- [14] C. M. Joyce and T. A. Steitz, Function and structure relationships in DNA polymerases, *Annu. Rev. Biochem.* **63**, 777 (1994).
- [15] M. K. Swan, R. E. Johnson, L. Prakash, S. Prakash, and A. K. Aggarwal, Structural basis of high fidelity DNA synthesis by yeast DNA polymerase delta, *Nat. Struct. Mol. Biol.* **16**, 979 (2009).
- [16] B. D. Freudenthal, W. A. Beard, D. D. Shock, and S. H. Wilson, Observing a DNA polymerase choose right from wrong, *Cell* **154**, 157 (2013).
- [17] T. Hunter, The genesis of tyrosine phosphorylation, *Cold Spring Harbor Perspect. Biol.* **6**, (2014).
- [18] M. B. Yaffe, Phosphotyrosine-binding domains in signal transduction, *Nat. Rev. Mol. Cell Biol.* **3**, 177 (2002).
- [19] B. T. Seet, I. Dikic, Z. Ming-Ming, and T. Pawson, Reading protein modifications with interaction domains, *Nat. Rev. Mol. Cell Biol.* **7**, 473 (2006).
- [20] W. A. Lim and T. Pawson, Phosphotyrosine signaling: Evolving a new cellular communication system, *Cell* **142**, 661 (2010).
- [21] J. A. Adams, Kinetic and catalytic mechanisms of protein kinases, *Chem. Rev.* **101**, 2271 (2001).
- [22] Madhusudan, P. Akamine, N.-H. Xuong, and S. S. Taylor, Crystal structure of a transition state mimic of the catalytic subunit of cAMP-dependent protein kinase, *Nat. Struct. Mol. Biol.* **9**, 273 (2002).
- [23] S. R. Hubbard, L. Wei, L. Ellis, and W. A. Hendrickson, Crystal structure of the tyrosine kinase domain of the human insulin receptor, *Nature (London)* **372**, 746 (1994).
- [24] D. Mahadevan, N. Thanki, P. McPhie, J. Beeler, J. Yu, A. Wlodawer, and M. Heidarani, Comparison of calcium-dependent conformational changes in the N-terminal SH2 domains of p85 and GAP defines distinct properties for SH2 domains, *Biochem.* **33**, 746 (1994).
- [25] J. Hutter, M. Iannuzzi, F. Schiffmann, and J. VandeVondele, CP2K: Atomistic simulations of condensed matter systems, *Wiley Interdiscip. Rev. Comput. Mol. Sci.* **4**, 15 (2014).
- [26] B. G. Lippert, J. H. Parrinello, and Michele, A hybrid Gaussian and plane wave density functional scheme, *Mol. Phys.* **92**, 477 (1997).
- [27] M. Iannuzzi and J. Hutter, Inner-shell spectroscopy by the Gaussian and augmented plane wave method, *Phys. Chem. Chem. Phys.* **9**, 1599 (2007).
- [28] J. VandeVondele, M. Krack, F. Mohamed, M. Parrinello, T. Chassaing, and J. Hutter, Quickstep: Fast and accurate density functional calculations using a mixed Gaussian and plane waves approach, *Comput. Phys. Commun.* **167**, 103 (2005).
- [29] S. Goedecker, M. Teter, and J. Hutter, Separable dual-space Gaussian pseudopotentials, *Phys. Rev. B* **54**, 1703 (1996).
- [30] Y. Zhang and W. Yang, Comment on “Generalized Gradient Approximation Made Simple”, *Phys. Rev. Lett.* **80**, 890 (1998).
- [31] S. Grimme, J. Antony, S. Ehrlich, and H. Krieg, A consistent and accurate ab initio parametrization of density functional dispersion correction (DFT-D) for the 94 elements H-Pu, *J. Chem. Phys.* **132**, 154104 (2010).
- [32] J. Schmidt, J. VandeVondele, I. F. Kuo, D. Sebastiani, J. I. Siepmann, J. Hutter, and C. J. Mundy, Isobaric-isothermal molecular dynamics simulations utilizing density functional theory: An assessment of the structure and density of water at near-ambient conditions, *J. Phys. Chem. B* **113**, 11959 (2009).
- [33] M. D. Baer, C. J. Mundy, M. J. Mcgrath, I. F. Kuo, J. I. Siepmann, and D. J. Tobias, Re-examining the properties of the aqueous vapor-liquid interface using dispersion corrected density functional theory, *J. Chem. Phys.* **135**, 124712 (2011).
- [34] Y. Ding, A. A. Hassanali, and M. Parrinello, Anomalous water diffusion in salt solutions, *Proc. Natl. Acad. Sci. USA* **111**, 3310 (2014).
- [35] M. Galib, M. Baer, L. Skinner, C. Mundy, T. Huthwelker, G. Schenter, C. Benmore, N. Govind, and J. Fulton, Revisiting the hydration structure of aqueous Na^+ , *J. Chem. Phys.* **146**, 084504 (2017).
- [36] A. D. Becke, Density-functional thermochemistry. III. The role of exact exchange, *J. Chem. Phys.* **98**, 5648 (1993).
- [37] M. Frisch, G. Trucks, H. B. Schlegel, G. Scuseria, M. Robb, J. Cheeseman, G. Scalmani, V. Barone, B. Mennucci, and G. Petersson, Gaussian 09, revision A.02, Gaussian, Inc, Wallingford, CT, 2009.
- [38] See Supplemental Material at <http://link.aps.org/supplemental/10.1103/PhysRevE.101.022410> for method details, movies, and additional figures.
- [39] A. S. Reddy, H. Zipse, and G. N. Sastry, Cation- π interactions of bare and coordinatively saturated metal ions: Contrasting structural and energetic characteristics, *J. Phys. Chem. B* **111**, 11546 (2007).
- [40] J. S. Rao, H. Zipse, and G. N. Sastry, Explicit solvent effect on cation- π interactions: A first principle investigation, *J. Phys. Chem. B* **113**, 7225 (2009).

- [41] A. S. Mahadevi and G. N. Sastry, Cation– π interaction: Its role and relevance in chemistry, biology, and material science, *Chem. Rev.* **113**, 2100 (2013).
- [42] J. C. Ma and D. A. Dougherty, The cation– π interaction, *Chem. Rev.* **97**, 1303 (1997).
- [43] A. K. Katz, J. P. Glusker, S. A. Beebe, and C. W. Bock, Calcium ion coordination: A comparison with that of beryllium, magnesium, and zinc, *J. Am. Chem. Soc.* **118**, 5752 (1996).
- [44] M. Harding, The geometry of metal-ligand interactions relevant to proteins, *Acta Crystallogr. D* **55**, 1432 (1999).
- [45] C. H. Chuang and Y. T. Chen, Raman scattering of L-tryptophan enhanced by surface plasmon of silver nanoparticles: Vibrational assignment and structural determination, *J. Raman Spectrosc.* **40**, 150 (2010).
- [46] G. Shi, Y. Dang, T. Pan, X. Liu, H. Liu, S. Li, L. Zhang, H. Zhao, S. Li, and J. Han, Unexpectedly Enhanced Solubility of Aromatic Amino Acids and Peptides in an Aqueous Solution of Divalent Transition-Metal Cations, *Phys. Rev. Lett.* **117**, 238102 (2016).
- [47] L. Chen, G. Shi, J. Shen, B. Peng, B. Zhang, Y. Wang, F. Bian, J. Wang, D. Li, and Z. Qian, Ion sieving in graphene oxide membranes via cationic control of interlayer spacing, *Nature (London)* **550**, 380 (2017).
- [48] H. Yorita, K. Otomo, H. Hiramatsu, A. Toyama, T. Miura, and H. Takeuchi, Evidence for the cation– π interaction between Cu^{2+} and tryptophan, *J. Am. Chem. Soc.* **130**, 15266 (2008).
- [49] J. Martin and B. P. Dailey, Proton NMR spectra of disubstituted benzenes, *J. Chem. Phys.* **37**, 2594 (1962).
- [50] M. Zanger, The determination of aromatic substitution patterns by nuclear magnetic resonance, *Org. Mag. Res.* **4**, 1 (1972).